Brain Structure and Function (2022) 227:763–778
https://doi.org/10.1007/s00429-021-02421-6

METHODS PAPER

An extended Human Connectome Project multimodal parcellation atlas of the human cortex and subcortical areas

Chu-Chung Huang[1] · Edmund T. Rolls[2,3,4] · Jianfeng Feng[2,3] · Ching-Po Lin[2,5,6]

Received: 29 July 2021 / Accepted: 25 October 2021 / Published online: 17 November 2021

Abstract

A modified and extended version, HCPex, is provided of the surface-based Human Connectome Project-MultiModal Parcellation atlas of human cortical areas (HCP-MMP v1.0, Glasser et al. 2016). The original atlas with 360 cortical areas has been modified in HCPex for ease of use with volumetric neuroimaging software, such as SPM, FSL, and MRIcroGL. HCPex is also an extended version of the original atlas in which 66 subcortical areas (33 in each hemisphere) have been added, including the amygdala, thalamus, putamen, caudate nucleus, nucleus accumbens, globus pallidus, mammillary bodies, septal nuclei and nucleus basalis. HCPex makes available the excellent parcellation of cortical areas in HCP-MMP v1.0 to users of volumetric software, such as SPM and FSL, as well as adding some subcortical regions, and providing labelled coronal views of the human brain.

Keywords Neuroimaging atlas · Human Connectome Project · HCPex · Extended HCP atlas · fMRI

Introduction

The Human Connectome Project multimodal parcellation atlas (HCP-MMP) provides a very useful parcellation of human cerebral cortical areas (Glasser et al. 2016a, b). The atlas is multimodal in that each region is defined by a combination of four criteria, architecture (T1w/T2w myelin content and cortical thickness maps), resting-state functional connectivity, task-based activation, and topographic organization, using a 3T MRI scanner (Glasser et al. 2016a). The HCP-MMP v1.0 atlas includes 180 cortical areas in each hemisphere, based on analyses in 210 participants. The areas defined include many areas that are of interest because of evidence on their functions, such as parieto-temporal cortex areas LIP, VIP, MT, MST, and occipital areas including V1, V2, V3, V4, etc. Given the usefulness of the parcellation provided in the HCP-MMP v1.0 atlas (Glasser et al. 2016a), we provide here a new extended version of the atlas, HCPex, that has the aim and rationale of making it more useful, by extending it by providing it in volumetric form, by adding 66 subcortical areas, and by providing a reordered version with an option to revert to the original order, as described below. We note that this atlas helps in the analysis of brain structure and function, for many of the cortical areas defined in the HCP atlas are known about functionally, and the atlas helps new investigations of the brain to be related to the known functions of those anatomically defined brain areas.

First, HCPex is provided in a volumetric form, which facilitates its use with software, such as SPM, FSL, FreeSurfer, and MRIcroGL, for which the necessary label files are provided. (The original HCP-MMP v1.0 atlas is available in the surface space of fsaverage (Glasser et al. 2016a). Some previous conversions to volumetric space have been

✉ Chu-Chung Huang
czhuang@psy.ecnu.edu.cn

✉ Edmund T. Rolls
Edmund.Rolls@oxcns.org
https://www.oxcns.org

1 Shanghai Key Laboratory of Brain Functional Genomics (Ministry of Education), Institute of Cognitive Neuroscience, School of Psychology and Cognitive Science, East China Normal University, Shanghai, China

2 Institute of Science and Technology for Brain Inspired Intelligence, Fudan University, Shanghai, China

3 Department of Computer Science, University of Warwick, Coventry CV4 7AL, UK

4 Oxford Centre for Computational Neuroscience, Oxford, UK

5 Institute of Neuroscience, National Yang-Ming Chiao Tung University, Taipei, Taiwan

6 Brain Research Center, National Yang-Ming Chiao Tung University, Taipei, Taiwan

provided (Horn 2016a, b; Coalson et al. 2018).) We provide the HCPex atlas in 1 mm and 2 mm versions, and provide a User Guide about how to install it with these types of software. Second, HCPex is extended beyond the 360 cortical areas of the HCP-MMP, to include in addition 66 subcortical areas (33 in each hemisphere), with the aim of making it more useful in many functional and structural connectome studies. Third, the brain areas in the atlas have been reordered in HCPex according to their cortical system, as the original order of labels of the HCP-MMP v1.0 atlas was not easy to follow for some users. However, we have ensured that either version of the ordering can be used, by providing a conversion function between the two orders. Fourth, to better visualize the atlas, we provide in this paper for HCPex coronal views of the brain with each HCPex area labelled to demonstrate the locations in the human brain of the 426 brain areas defined in this atlas. This is proving to be a very helpful addition for users. This HCPex extended atlas has already proved useful in tractography (Huang et al. 2021), functional connectivity (Ma et al. 2021), and effective connectivity (Rolls et al. 2021) analysis of the human hippocampal memory system.

We note that surface-based registration such as that provided by the HCP-MMP v1.0 leads to better spatial localization of cortical areas than volumetric methods (Glasser et al. 2016b; Coalson et al. 2018) such as those commonly used and made available in neuroimaging software, such as SPM (Friston et al. 2006) (https://www.fil.ion.ucl.ac.uk/spm/) and FSL (Smith et al. 2004; Jenkinson et al. 2012) (https://fsl.fmrib.ox.ac.uk/). However, given that much neuroimaging analysis is performed with software such as SPM and FSL, and that volumetric analysis enables subcortical areas to be easily included straightforwardly in the atlas which is an aim of HCPex, we have provided HCPex. At the same time, where better localization is required than may be provided with HCPex, we appreciate and recommend the use of the surface-based version HCP-MMP v1.0 (Glasser et al. 2016a), for the reasons set out by Coalson et al (2018). We are very impressed by the parcellation provided in the HCP-MMP atlas (Glasser et al. 2016a), and that is a reason why we have used HCPex in analyses that includes subcortical areas (Huang et al. 2021; Ma et al. 2021; Rolls et al. 2021), and also a reason for making HCPex available for use by others. As HCPex has its foundation in HCP-MMP v1.0, we recommend that Glasser et al (2016a) is cited when HCPex is used in published research. We note that FreeSurfer (Fischl et al. 1999a, b) (http://surfer.nmr.mgh.harvard.edu/) does utilise surface-based registration, but provides only a limited number of subcortical regions. We provide HCPex therefore with the aim of making the excellent parcellation of the cortex provided in HCP-MMP v1.0 available in a volumetric form that includes also some subcortical areas and that is suitable for use with software such as SPM and FSL. At the same time, we recommend the surface-based version of HCP-MMP v1.0 (Glasser et al. 2016a) for use when more accurate registration is needed (Coalson et al. 2018).

Methods

Overview

The definition of regions in the Human Connectome Project (HCP) atlas is shown in Glasser_2016_Table.xlsx of Glasser et al. (2016a, b). A list of these regions is provided in Table 1, and in Fig. 1, we show coronal slices with labels for the regions defined in the HCPex atlas. The cortical regions in Fig. 1 were as defined in the Human Connectome Project (HCP) atlas (Glasser et al. 2016a).

The extended atlas described here combines the following regions: HCP's multi-modal parcellation (v1.0), consisting of 180 regions per hemisphere (Glasser et al. 2016a); 21 thalamic nuclei; and 12 other subcortical regions, including the amygdala, putamen, caudate nucleus, nucleus accumbens, globus pallidus externalis, globus pallidus internalis, substantia nigra pars compacta, substantia nigra pars reticulata, ventral tegmental area, mammillary bodies, the septal nuclei and the nucleus basalis. The subcortical regions are listed in Table 2, and are also shown in Fig. 1.

The original HCP atlas was made using the multimodal surface matching (MSM) approach (Glasser et al. 2016a), that registered participants' multiple-modal images onto surface space, and is not in the standard volumetric MNI152 space that is commonly used in neuroscience research. Mills (2016) and Beauchamp (2021) mapped the HCP-MMP1 atlas into the volumetric MNI152 template brain by a transformation from the multimodal surface matching format (MSM, the algorithm utilized in the original HCP atlas) to the ICBM 2009c asymmetric template based on 152 participants (Fonov et al. 2009, 2011). To convert the parcellation from the HCP-MMP1 surface space to the MNI152 volumetric space, they performed the following steps: (1) Connectome Workbench was used to convert the atlas from CIFTI to GIFTI format. (2) Parcellation in GIFTI format was then resampled to FreeSurfer fsaverage space based on the standard mesh sphere. (3) The FreeSurfer command line: "mris_convert" was used to transform the parcellation from GIFTI format to annotation files. (4) A surface-based version of the atlas was produced from the MNI152 ICBM 2009c asymmetric T1 volumetric image. (5) Surface-based registration was then applied to register between the fsaverage and surface space version of ICBM 2009c. (6) The HCP-MMP1 annotation file was converted from the fsaverage to ICBM 2009c. (7) The HCP-MMP1 annotation in ICBM 2009c space was then converted to the volume space of the ICBM 2009c template. Detailed information about

Table 1 The list of the reordered cortical regions of the HCPex atlas

Reordered ID (L, R)	Region	RegionLongName	Cortical Division	Cortex ID	Original ID	Voxel numbers (1 mm^3) (L,R)
1, 181	V1	Primary_Visual_Cortex	Primary_Visual	1	1	13,812, 13,406
2, 182	V2	Second_Visual_Area	Early_Visual	2	4	9515, 9420
3, 183	V3	Third_Visual_Area	Early_Visual	2	5	7106, 7481
4, 184	V4	Fourth_Visual_Area	Early_Visual	2	6	4782, 4537
5, 185	IPS1	IntraParietal_Sulcus_Area_1	Dorsal_Stream_Visual	3	17	1751, 1750
6, 186	V3A	Area_V3A	Dorsal_Stream_Visual	3	13	2191, 2212
7, 187	V3B	Area_V3B	Dorsal_Stream_Visual	3	19	639, 731
8, 188	V6	Sixth_Visual_Area	Dorsal_Stream_Visual	3	3	1402, 1559
9, 189	V6A	Area_V6A	Dorsal_Stream_Visual	3	152	904, 734
10, 190	V7	Seventh_Visual_Area	Dorsal_Stream_Visual	3	16	1005, 1041
11, 191	FFC	Fusiform_Face_Complex	Ventral_Stream_Visual	4	18	3848, 4402
12, 192	PIT	Posterior_InferoTemporal_complex	Ventral_Stream_Visual	4	22	1392, 1386
13, 193	V8	Eighth_Visual_Area	Ventral_Stream_Visual	4	7	1361, 1175
14, 194	VMV1	VentroMedial_Visual_Area_1	Ventral_Stream_Visual	4	153	939, 1219
15, 195	VMV2	VentroMedial_Visual_Area_2	Ventral_Stream_Visual	4	160	639, 923
16, 196	VMV3	VentroMedial_Visual_Area_3	Ventral_Stream_Visual	4	154	941, 1242
17, 197	VVC	Ventral_Visual_Complex	Ventral_Stream_Visual	4	163	2487, 2753
18, 198	FST	Area_FST	MT + _Complex	5	157	1324, 1683
19, 199	LO1	Area_Lateral_Occipital_1	MT + _Complex	5	20	619, 909
20, 200	LO2	Area_Lateral_Occipital_2	MT + _Complex	5	21	1179, 1062
21, 201	LO3	Area_Lateral_Occipital_3	MT + _Complex	5	159	438, 915
22, 202	MST	Medial_Superior_Temporal_Area	MT + _Complex	5	2	794, 1036
23, 203	MT	Middle_Temporal_Area	MT + _Complex	5	23	620, 1005
24, 204	PH	Area_PH	MT + _Complex	5	138	3453, 3205
25, 205	V3CD	Area_V3CD	MT + _Complex	5	158	876, 1222
26, 206	V4t	Area_V4t	MT + _Complex	5	156	1037, 1249
27, 207	1	Area_1	SomaSens_Motor	6	51	6590, 5925
28, 208	2	Area_2	SomaSens_Motor	6	52	4278, 4727
29, 209	3a	Area_3a	SomaSens_Motor	6	53	2247, 2286
30, 210	3b	Primary_Sensory_Cortex	SomaSens_Motor	6	9	5451, 4350
31, 211	4	Primary_Motor_Cortex	SomaSens_Motor	6	8	10,776, 10,254
32, 212	23c	Area_23c	ParaCentral_MidCing	7	38	2259, 2498
33, 213	24dd	Dorsal_Area_24d	ParaCentral_MidCing	7	40	2665, 2820
34, 214	24dv	Ventral_Area_24d	ParaCentral_MidCing	7	41	1076, 1349
35, 215	5L	Area_5L	ParaCentral_MidCing	7	39	2249, 2327
36, 216	5 m	Area_5m	ParaCentral_MidCing	7	36	1483, 2079
37, 217	5mv	Area_5m_ventral	ParaCentral_MidCing	7	37	1651, 1996
38, 218	6ma	Area_6m_anterior	ParaCentral_MidCing	7	44	3941, 4251
39, 219	6mp	Area_6mp	ParaCentral_MidCing	7	55	3701, 3105
40, 220	SCEF	Supplementary_and_Cingulate_Eye_Field	ParaCentral_MidCing	7	43	3500, 3371
41, 221	55b	Area_55b	Premotor	8	12	2422, 1537
42, 222	6a	Area_6_anterior	Premotor	8	96	4233, 3752
43, 223	6d	Dorsal_area_6	Premotor	8	54	2916, 2909
44, 224	6r	Rostral_Area_6	Premotor	8	78	3029, 3981
45, 225	6v	Ventral_Area_6	Premotor	8	56	2075, 2516
46, 226	FEF	Frontal_Eye_Fields	Premotor	8	10	1787, 1889
47, 227	PEF	Premotor_Eye_Field	Premotor	8	11	1006, 1258
48, 228	43	Area_43	Posterior_Opercular	9	99	1889, 1678
49, 229	FOP1	Frontal_Opercular_Area_1	Posterior_Opercular	9	113	879, 932

Table 1 (continued)

Reordered ID (L, R)	Region	RegionLongName	Cortical Division	Cortex ID	Original ID	Voxel numbers (1 mm^3) (L,R)
50, 230	OP1	Area_OP1-SII	Posterior_Opercular	9	101	1275, 1072
51, 231	OP2-3	Area_OP2-3-VS	Posterior_Opercular	9	102	943, 792
52, 232	OP4	Area_OP4-PV	Posterior_Opercular	9	100	2332, 2409
53, 233	52	Area_52	Early_Auditory	10	103	725, 580
54, 234	A1	Primary_Auditory_Cortex	Early_Auditory	10	24	1023, 796
55, 235	LBelt	Lateral_Belt_Complex	Early_Auditory	10	174	820, 901
56, 236	MBelt	Medial_Belt_Complex	Early_Auditory	10	173	1242, 1236
57, 237	PBelt	ParaBelt_Complex	Early_Auditory	10	124	1719, 1439
58, 238	PFcm	Area_PFcm	Early_Auditory	10	105	1486, 1485
59, 239	RI	RetroInsular_Cortex	Early_Auditory	10	104	1149, 1334
60, 240	A4	Auditory_4_Complex	Auditory_Association	11	175	3514, 3610
61, 241	A5	Auditory_5_Complex	Auditory_Association	11	125	3346, 3881
62, 242	STGa	Area_STGa	Auditory_Association	11	123	2509, 2187
63, 243	STSda	Area_STSd_anterior	Auditory_Association	11	128	1944, 2389
64, 244	STSdp	Area_STSd_posterior	Auditory_Association	11	129	1994, 2605
65, 245	STSva	Area_STSv_anterior	Auditory_Association	11	176	1694, 1900
66, 246	STSvp	Area_STSv_posterior	Auditory_Association	11	130	2898, 2515
67, 247	TA2	Area_TA2	Auditory_Association	11	107	1518, 1726
68, 248	AAIC	Anterior_Agranular_Insula_Complex	Insula_FrontalOperc	12	112	1859, 1691
69, 249	AVI	Anterior_Ventral_Insular_Area	Insula_FrontalOperc	12	111	1446, 1792
70, 250	FOP2	Frontal_Opercular_Area_2	Insula_FrontalOperc	12	115	750, 720
71, 251	FOP3	Frontal_Opercular_Area_3	Insula_FrontalOperc	12	114	754, 614
72, 252	FOP4	Frontal_Opercular_Area_4	Insula_FrontalOperc	12	108	2522, 1678
73, 253	FOP5	Area_Frontal_Opercular_5	Insula_FrontalOperc	12	169	1297, 1365
74, 254	Ig	Insular_Granular_Complex	Insula_FrontalOperc	12	168	841, 1077
75, 255	MI	Middle_Insular_Area	Insula_FrontalOperc	12	109	2102, 1960
76, 256	PI	Para-Insular_Area	Insula_FrontalOperc	12	178	1033, 1058
77, 257	Pir	Pirform_Cortex	Insula_FrontalOperc	12	110	2287, 1856
78, 258	PoI1	Area_Posterior_Insular_1	Insula_FrontalOperc	12	167	1811, 1835
79, 259	PoI2	Posterior_Insular_Area_2	Insula_FrontalOperc	12	106	2747, 2675
80, 260	H	Hippocampus	Medial_Temporal	13	120	4283, 3626
81, 261	PreS	PreSubiculum	Medial_Temporal	13	119	1817, 1558
82, 262	EC	Entorhinal_Cortex	Medial_Temporal	13	118	2127, 2110
83, 263	PeEc	Perirhinal_Ectorhinal_Cortex	Medial_Temporal	13	122	4826, 4755
84, 264	TF	Area_TF	Medial_Temporal	13	135	3986, 4752
85, 265	PHA1	ParaHippocampal_Area_1	Medial_Temporal	13	126	1281, 1168
86, 266	PHA2	ParaHippocampal_Area_2	Medial_Temporal	13	155	783, 771
87, 267	PHA3	ParaHippocampal_Area_3	Medial_Temporal	13	127	2023, 1122
88, 268	PHT	Area_PHT	Lateral_Temporal	14	137	4182, 3410
89, 269	TE1a	Area_TE1_anterior	Lateral_Temporal	14	132	5227, 4180
90, 270	TE1m	Area_TE1_Middle	Lateral_Temporal	14	177	3339, 3429
91, 271	TE1p	Area_TE1_posterior	Lateral_Temporal	14	133	7116, 6010
92, 272	TE2a	Area_TE2_anterior	Lateral_Temporal	14	134	5691, 5753
93, 273	TE2p	Area_TE2_posterior	Lateral_Temporal	14	136	4115, 3040
94, 274	TGd	Area_TG_dorsal	Lateral_Temporal	14	131	10,192, 10,269
95, 275	TGv	Area_TG_Ventral	Lateral_Temporal	14	172	3694, 4515
96, 276	PSL	PeriSylvian_Language_Area	TPO	15	25	2154, 2759
97, 277	STV	Superior_Temporal_Visual_Area	TPO	15	28	2322, 2294
98, 278	TPOJ1	Area_TemporoParietoOccipital_Junction_1	TPO	15	139	2102, 3938

Table 1 (continued)

Reordered ID (L, R)	Region	RegionLongName	Cortical Division	Cortex ID	Original ID	Voxel numbers (1 mm^3) (L,R)
99, 279	TPOJ2	Area_TemporoParietoOccipital_Junction_2	TPO	15	140	1930, 2068
100, 280	TPOJ3	Area_TemporoParietoOccipital_Junction_3	TPO	15	141	1290, 1277
101, 281	7AL	Lateral_Area_7A	Superior_Parietal	16	42	2134, 2030
102, 282	7Am	Medial_Area_7A	Superior_Parietal	16	45	2995, 2379
103, 283	7PC	Area_7PC	Superior_Parietal	16	47	3151, 3415
104, 284	7Pl	Lateral_Area_7P	Superior_Parietal	16	46	1695, 1363
105, 285	7Pm	Medial_Area_7P	Superior_Parietal	16	29	1601, 1308
106, 286	AIP	Anterior_IntraParietal_Area	Superior_Parietal	16	117	1999, 2542
107, 287	LIPd	Area_Lateral_IntraParietal_dorsal	Superior_Parietal	16	95	1008, 869
108, 288	LIPv	Area_Lateral_IntraParietal_ventral	Superior_Parietal	16	48	1681, 1783
109, 289	MIP	Medial_IntraParietal_Area	Superior_Parietal	16	50	1872, 2403
110, 290	VIP	Ventral_IntraParietal_Complex	Superior_Parietal	16	49	1890, 1577
111, 291	IP0	Area_IntraParietal_0	Inferior_Parietal	17	146	1203, 1239
112, 292	IP1	Area_IntraParietal_1	Inferior_Parietal	17	145	1692, 1632
113, 293	IP2	Area_IntraParietal_2	Inferior_Parietal	17	144	2102, 1861
114, 294	PF	Area_PF_Complex	Inferior_Parietal	17	148	5457, 5251
115, 295	PFm	Area_PFm_Complex	Inferior_Parietal	17	149	8220, 8141
116, 296	PFop	Area_PF_Opercular	Inferior_Parietal	17	147	1797, 1783
117, 297	PFt	Area_PFt	Inferior_Parietal	17	116	1983, 2039
118, 298	PGi	Area_PGi	Inferior_Parietal	17	150	4791, 4970
119, 299	PGp	Area_PGp	Inferior_Parietal	17	143	2501, 3740
120, 300	PGs	Area_PGs	Inferior_Parietal	17	151	4552, 3366
121, 301	23d	Area_23d	Posterior_Cingulate	18	32	1261, 1513
122, 302	31a	Area_31a	Posterior_Cingulate	18	162	1260, 1116
123, 303	31pd	Area_31pd	Posterior_Cingulate	18	161	1428, 864
124, 304	31pv	Area_31p_ventral	Posterior_Cingulate	18	35	950, 1022
125, 305	7 m	Area_7m	Posterior_Cingulate	18	30	2128, 2067
126, 306	d23ab	Area_dorsal_23_a + b	Posterior_Cingulate	18	34	1607, 1106
127, 307	DVT	Dorsal_Transitional_Visual_Area	Posterior_Cingulate	18	142	1806, 2176
128, 308	PCV	PreCuneus_Visual_Area	Posterior_Cingulate	18	27	2245, 2416
129, 309	POS1	Parieto-Occipital_Sulcus_Area_1	Posterior_Cingulate	18	31	2531, 2727
130, 310	POS2	Parieto-Occipital_Sulcus_Area_2	Posterior_Cingulate	18	15	3261, 3093
131, 311	ProS	ProStriate_Area	Posterior_Cingulate	18	121	1222, 1055
132, 312	RSC	RetroSplenial_Complex	Posterior_Cingulate	18	14	2830, 3067
133, 313	v23ab	Area_ventral_23_a + b	Posterior_Cingulate	18	33	916, 1089
134, 314	10r	Area_10r	AntCing_MedPFC	19	65	1589, 1053
135, 315	10v	Area_10v	AntCing_MedPFC	19	88	3906, 2667
136, 316	25	Area_25	AntCing_MedPFC	19	164	1911, 2135
137, 317	33pr	Area_33_prime	AntCing_MedPFC	19	58	1354, 1316
138, 318	8BM	Area_8BM	AntCing_MedPFC	19	63	3122, 3436
139, 319	9 m	Area_9_Middle	AntCing_MedPFC	19	69	6338, 5881
140, 320	a24	Area_a24	AntCing_MedPFC	19	61	2085, 2152
141, 321	a24pr	Anterior_24_prime	AntCing_MedPFC	19	59	1095, 1474
142, 322	a32pr	Area_anterior_32_prime	AntCing_MedPFC	19	179	1759, 1118
143, 323	d32	Area_dorsal_32	AntCing_MedPFC	19	62	2228, 2374
144, 324	p24	Area_posterior_24	AntCing_MedPFC	19	180	2394, 2442
145, 325	p24pr	Area_Posterior_24_prime	AntCing_MedPFC	19	57	1422, 1724
146, 326	p32	Area_p32	AntCing_MedPFC	19	64	1180, 1765
147, 327	p32pr	Area_p32_prime	AntCing_MedPFC	19	60	1569, 1305

Table 1 (continued)

Reordered ID (L, R)	Region	RegionLongName	Cortical Division	Cortex ID	Original ID	Voxel numbers (1 mm^3) (L,R)
148, 328	pOFC	Posterior_OFC_Complex	AntCing_MedPFC	19	166	2486, 2836
149, 329	s32	Area_s32	AntCing_MedPFC	19	165	604, 1015
150, 330	10d	Area_10d	OrbPolaFrontal	20	72	3644, 3096
151, 331	10 pp	Polar_10p	OrbPolaFrontal	20	90	1997, 2487
152, 332	11 l	Area_11l	OrbPolaFrontal	20	91	3531, 3793
153, 333	13 l	Area_13l	OrbPolaFrontal	20	92	2429, 1757
154, 334	47 m	Area_47m	OrbPolaFrontal	20	66	799, 781
155, 335	47 s	Area_47s	OrbPolaFrontal	20	94	2795, 3080
156, 336	a10p	Area_anterior_10p	OrbPolaFrontal	20	89	1964, 1748
157, 337	OFC	Orbital_Frontal_Complex	OrbPolaFrontal	20	93	4560, 5232
158, 338	p10p	Area_posterior_10p	OrbPolaFrontal	20	170	2116, 2365
159, 339	44	Area_44	Inferior_Frontal	21	74	2435, 2589
160, 340	45	Area_45	Inferior_Frontal	21	75	3762, 2962
161, 341	47 l	Area_47l_(47_lateral)	Inferior_Frontal	21	76	2527, 2592
162, 342	a47r	Area_anterior_47r	Inferior_Frontal	21	77	4167, 3763
163, 343	IFJa	Area_IFJa	Inferior_Frontal	21	79	1513, 1405
164, 344	IFJp	Area_IFJp	Inferior_Frontal	21	80	960, 740
165, 345	IFSa	Area_IFSa	Inferior_Frontal	21	82	2057, 2641
166, 346	IFSp	Area_IFSp	Inferior_Frontal	21	81	1589, 1730
167, 347	p47r	Area_posterior_47r	Inferior_Frontal	21	171	2133, 1761
168, 348	46	Area_46	Dorsolateral_Prefrontal	22	84	4863, 4394
169, 349	8Ad	Area_8Ad	Dorsolateral_Prefrontal	22	68	3386, 3492
170, 350	8Av	Area_8Av	Dorsolateral_Prefrontal	22	67	4807, 5902
171, 351	8BL	Area_8B_Lateral	Dorsolateral_Prefrontal	22	70	3377, 4078
172, 352	8C	Area_8C	Dorsolateral_Prefrontal	22	73	4085, 3134
173, 353	9-46d	Area_9-46d	Dorsolateral_Prefrontal	22	86	4534, 4666
174, 354	9a	Area_9_anterior	Dorsolateral_Prefrontal	22	87	3706, 3048
175, 355	9p	Area_9_Posterior	Dorsolateral_Prefrontal	22	71	3426, 2488
176, 356	a9-46v	Area_anterior_9-46v	Dorsolateral_Prefrontal	22	85	3314, 2628
177, 357	i6-8	Inferior_6-8_Transitional_Area	Dorsolateral_Prefrontal	22	97	1764, 2418
178, 358	p9-46v	Area_posterior_9-46v	Dorsolateral_Prefrontal	22	83	2871, 4635
179, 359	s6-8	Superior_6-8_Transitional_Area	Dorsolateral_Prefrontal	22	98	1336, 2132
180, 360	SFL	Superior_Frontal_Language_Area	Dorsolateral_Prefrontal	22	26	3873, 3055

Column 1 (Reordered ID) shows the order in HCPex based on the HCP-MMP1_UniqueRegionList.csv, as described in the Methods, of the 360 cortical regions originally defined by Glasser et al. (2016a, b). The names of the cortical divisions shown in column 4 come from the same.csv file. The sixth column shows the original order used by Glasser et al (2016a)

L left hemisphere, *R* right, *MT+_Complex* MT+_Complex_and_Neighboring_Visual_Areas, *SomaSens_Motor* Somatosensory_and_Motor, *ParaCentral_MidCing* Paracentral_Lobular_and_Mid_Cingulate, *Insula_FrontalOperc* Insular_and_Frontal_Opercular, *TPO* Temporo-Parieto-Occipital_Junction, *AntCing_MedPFC*, Anterior_Cingulate_and_Medial_Prefrontal, *OrbPolaFrontal* Orbital_and_Polar_Frontal

the processing steps and codes are described by Mills (2016) and Beauchamp (2021) (https://openwetware.org/wiki/Beauchamp:CorticalSurfaceHCP). The volumetric HCP-MMP1 atlas defined in the asymmetric MNI space of ICBM 2009c (Fonov et al. 2009, 2011) produced as just described can be found at the AFNI website (https://afni.nimh.nih.gov/pub/dist/atlases/MNI_HCP/).

In the HCP-MMP1 atlas, each region has its RegionID, which we show in Table 1 (column 6). Detailed information about the regions is available in the Supplementary Material File NIHMS68870-supplement-Neuroanatomical_Supplementary_Results.pdf provided by Glasser et al (2016a). In that Supplementary Material file, a grouping of the regions is suggested based on geographic proximity and functional similarities, and this grouping is shown in the columns labelled Cortical Divisions and Cortex ID that has led to a different ordering of the regions. In this modified version HCPex of the HCP-MMP atlas, we reordered the regions

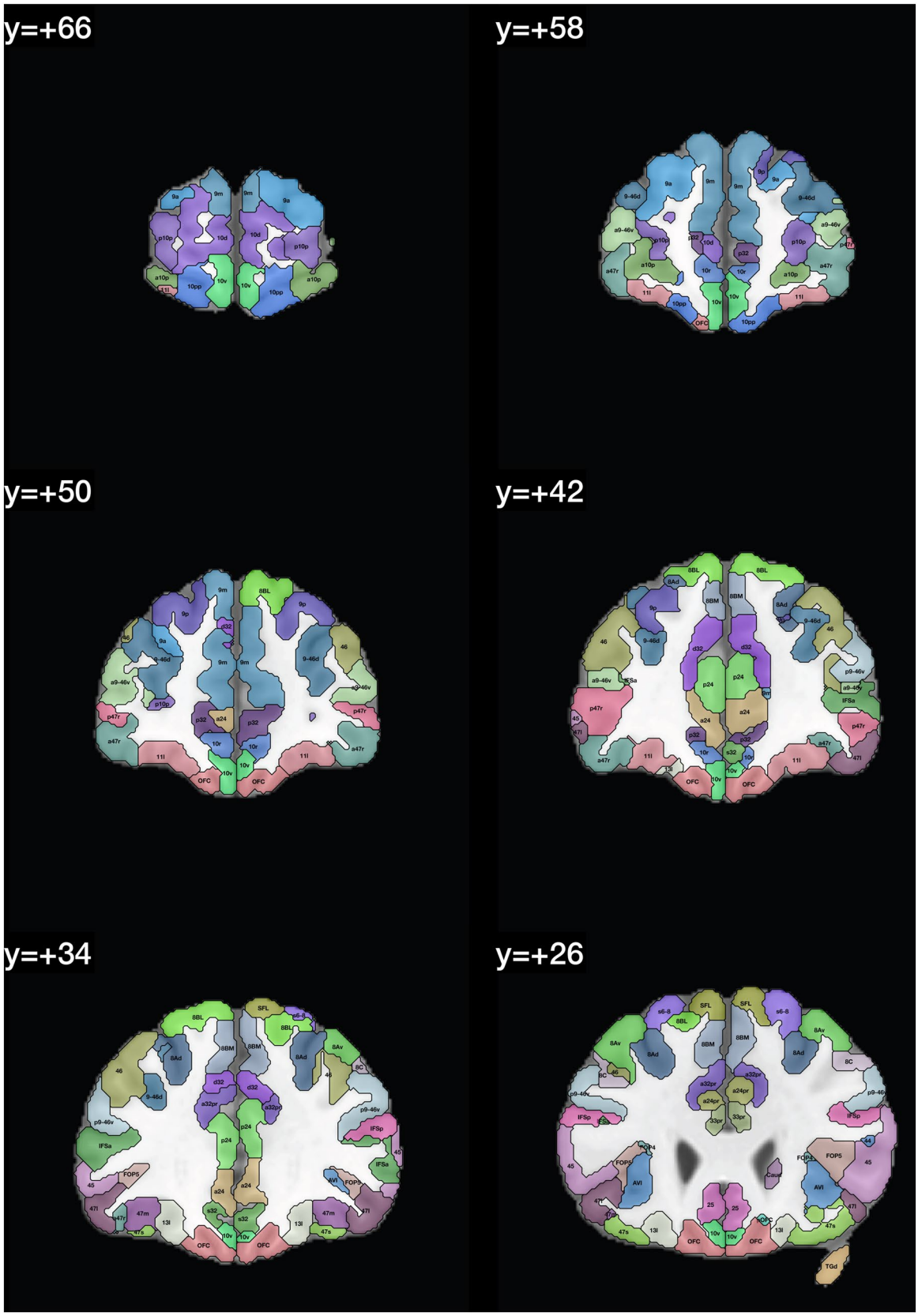

Fig. 1 Example coronal slices showing regions defined in the HCPex atlas and added subcortical regions. The abbreviations are as in Table 1. The *y* values for the coronal slices are in MNI coordinates

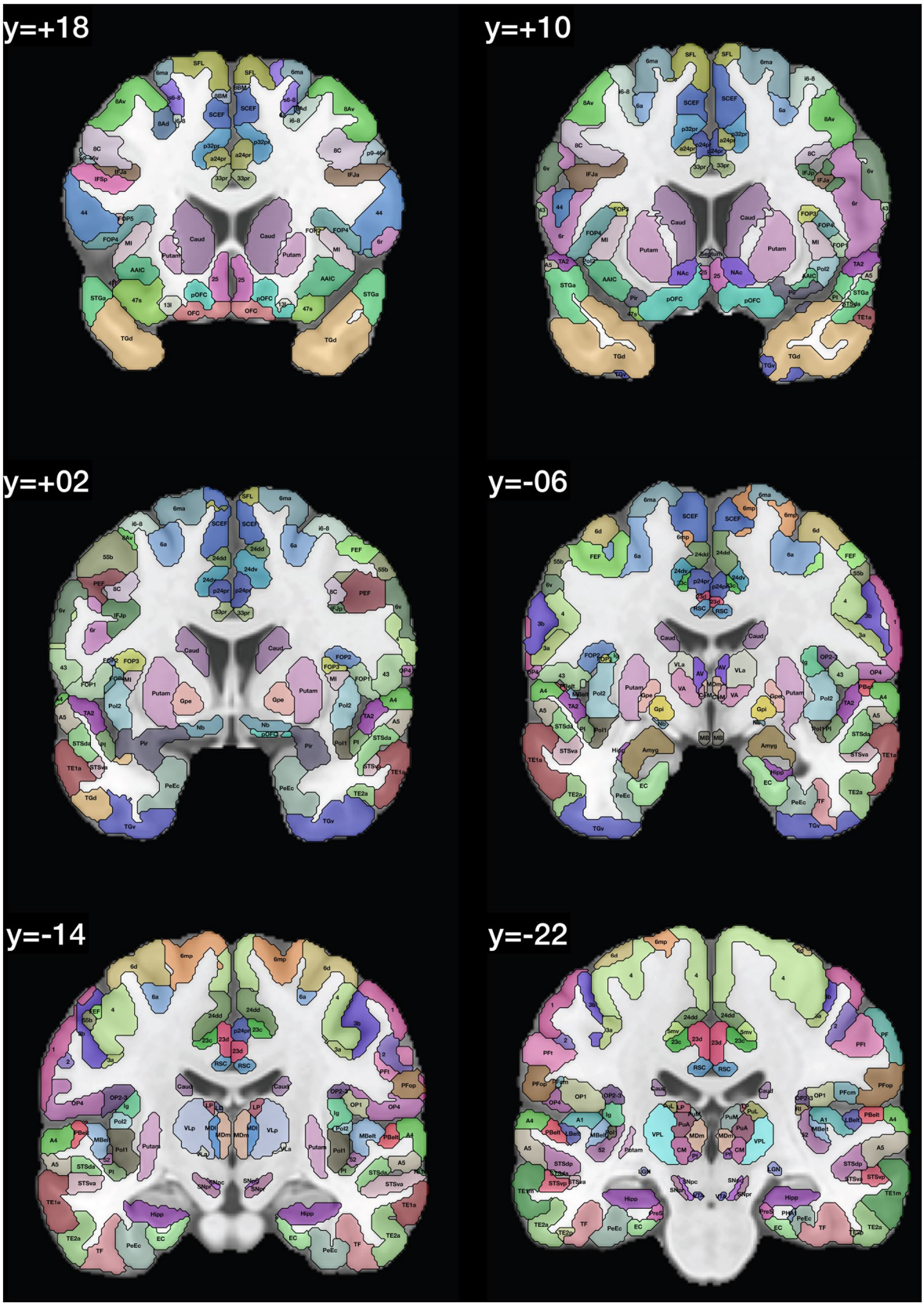

Fig. 1 (continued)

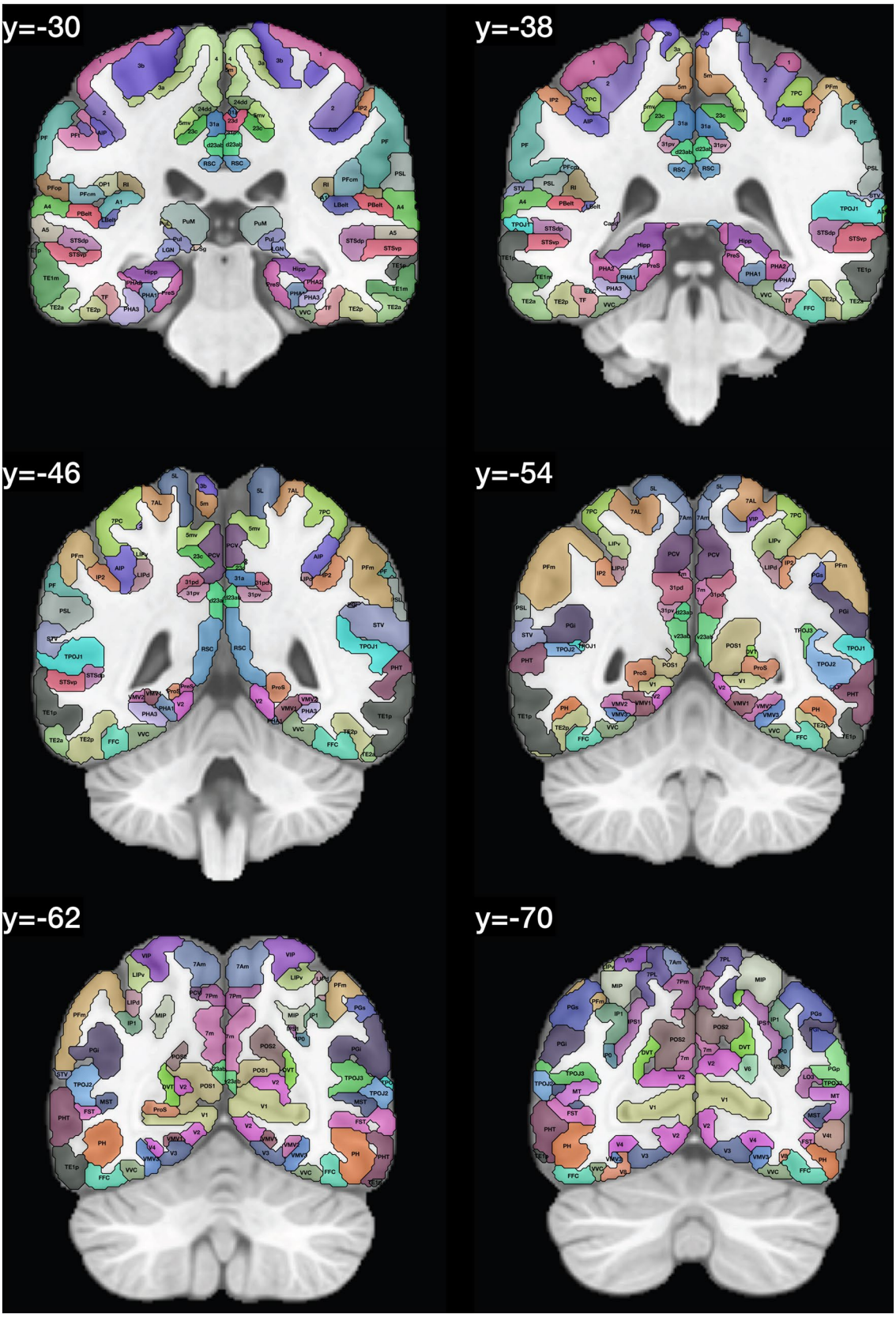

Fig. 1 (continued)

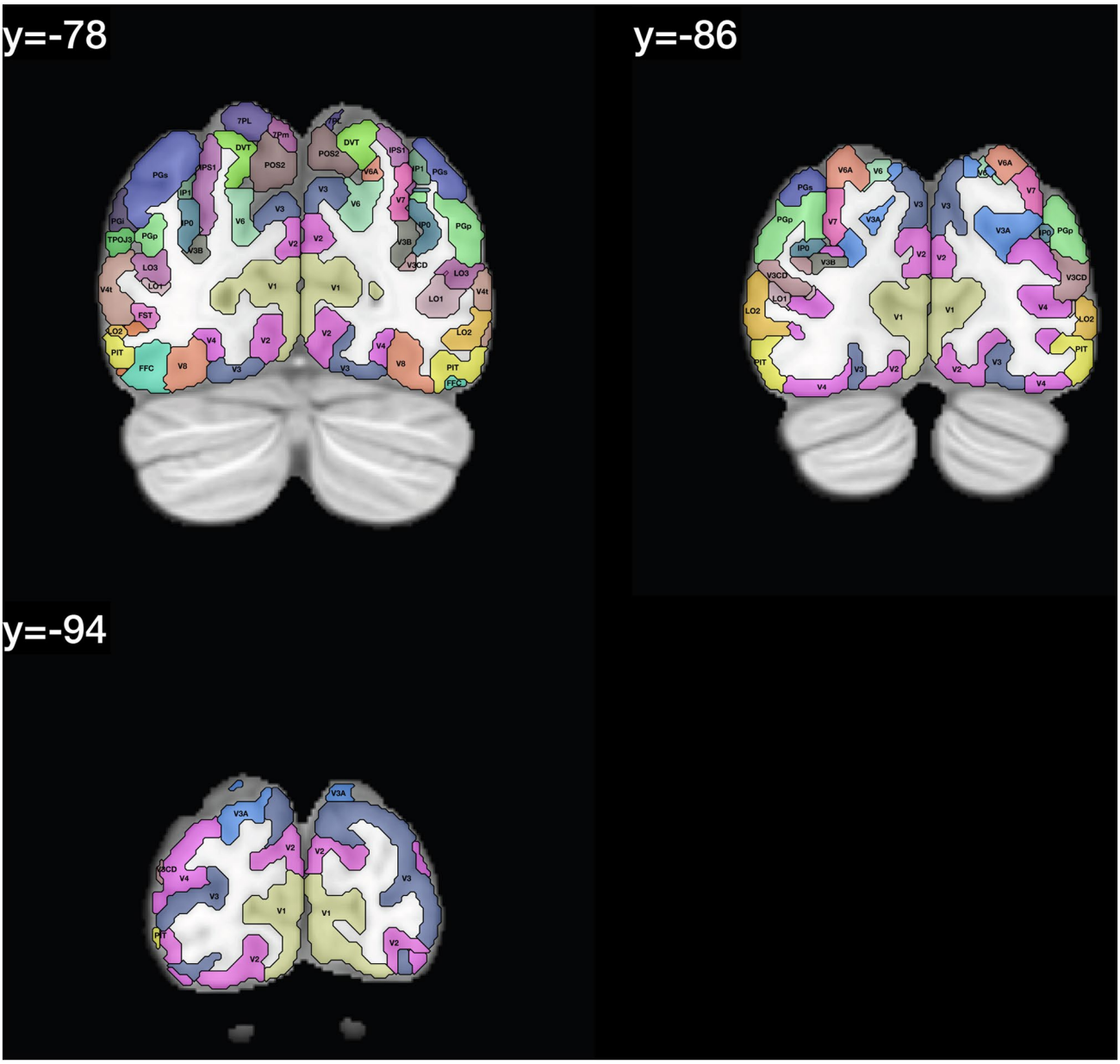

Fig. 1 (continued)

based on the Cortex ID described by Dr. Dianne Patterson of the University of Arizona at https://neuroimaging-core-docs.readthedocs.io/en/latest/pages/atlases.html in the file HCP-MMP1_UniqueRegionList.csv. Table 1 shows the reordered ID of each of the 360 original areas defined in the HCPMMP v1.0 atlas (180 in each hemisphere), along with the abbreviated name, the full name of the cortical area, Cortex Division, Cortex ID, original ID from the Glasser et al (2016a) paper, and the number of voxels. Table 2 shows the extended 66 subcortical regions (33 in each hemisphere) and their definitions.

To further facilitate the use of the HCPex atlas with different software, we resampled the atlas into low-resolution standard MNI152 space by performing rigid-body (with 6 *df*) registration between the skull-stripped MNI152 T1 2 mm isotropic T1 template and the ICBM 2009c asymmetric T1 template using Advanced Normalization Tools (Avants et al. 2009).

Table 2 The list of the subcortical regions in the atlas

ID (L,R)	Abbreviation	Full name	Voxel numbers (1 mm^3) (L, R)
361, 394	AV	Thalamus: Anteroventral Nucleus	256, 280
362, 395	CeM	Thalamus: Central medial	96, 88
363, 396	CL	Thalamus: Central lateral	16, 16
364, 397	CM	Thalamus: Centralmedian	424, 376
365, 398	LD	Thalamus: Laterodorsal	48, 8
366, 399	LGN	Thalamus: Lateral Geniculate	328, 256
367, 400	LP	Thalamus: Lateral Posterior	256, 264
368, 401	L-Sg	Thalamus: Limitans Suprageniculate	32, 16
369, 402	MDl	Thalamus: Mediodorsolateral parvocellular	328, 320
370, 403	MDm	Thalamus: Mediodorsomedial magnocellular	1104, 1192
371, 404	MGN	Thalamus: Medial Geniculate	160, 168
372, 405	MV(Re)	Thalamus: Reuniens	8, 8
373, 406	Pf	Thalamus: Parafascicular	56, 72
374, 407	PuA	Thalamus: Pulvinar anterior	320, 280
375, 408	PuI	Thalamus: Pulvinar inferior	336, 280
376, 409	PuL	Thalamus: Pulvinar lateral	304, 256
377, 410	PuM	Thalamus: Pulvinar medial	1904, 1680
378, 411	VA	Thalamus: Ventral Anterior	608, 616
379, 412	VLa	Thalamus: Ventral Lateral Anterior	880, 856
380, 413	VLp	Thalamus: Ventral Lateral Posterior	1384, 1288
381, 414	VPL	Thalamus: Ventral posterolateral	1600, 1368
382, 415	Putam	Putamen	7896, 7744
383, 416	Caud	Caudate	6896, 6952
384, 417	NAc	Nucleus Accumbens	600, 632
385, 418	Gpe	Globus pallidus externalis	1232, 1144
386, 419	Gpi	Globus pallidus internalis	632, 624
387, 420	Amyg	Amygdala	1608, 1632
388, 421	SNpc	Substantia nigra pars compacta	184, 200
389, 422	SNpr	Substantia nigra pars reticulata	408, 440
390, 423	VTA	Ventral tegmental area	40, 48
391, 424	MB	Mammillary bodies	112, 104
392, 425	Septum	Septal nuclei	248, 136
393, 426	Nb	Nucleus basalis	584, 600

Description of the new areas in the modified HCPMMP

A total of 66 new subcortical regions (33 in each hemisphere) were added to the modified HCP-MMP1 atlas. A list of the newly added subcortical parcellations is provided (Table 2). The new subcortical areas in the HCPex atlas run from ID 361 to 426 (left: 361–393, right: 394–426). The new subcortical areas are 21 thalamic nuclei (361–381, 394–414), putamen (382, 415), caudate (383, 416), nucleus accumbens (384, 417), globus pallidus externalis/internalis (385–386, 418–419), amygdala (387, 420), substantia nigra pars compacta/reticulata (388–389, 421–422), ventral tegmental area (390, 423), and mammillary bodies (391, 424), and the cholinergic nuclei: septal nuclei (392, 425) and the nucleus basalis (393, 426). All of the cortical and subcortical regions are registered to the standard space defined by the MNI space using the ICBM 2009c asymmetric template. The definitions of the subcortical areas are described in the next sections.

Amygdala

High-resolution amygdala segmentation was adapted from the Computational Brain Anatomy Lab Merged Atlas (CoBrALab, https://github.com/CoBrALab/atlases) (Entis et al. 2012; Pipitone et al. 2014). The subcortical regions in the CoBrALab atlas were manually delineated based on five high-resolution T1 and T2 templates, and the defined segmentations were applied to the Multiple Automatically

Generated Templates (MAGeT) pipeline to provide common-space localization in MNI standard space (Chakravarty et al. 2013). The segmentation of the amygdala (Treadway et al. 2015) is in the same MNI ICBM 2009c nonlinear asymmetric T1 space (Fonov et al. 2009, 2011) as HCPex.

Thalamic nuclei

The thalamic nuclei were segmented based on the customized module described in Iglesias et al (2018), which is a Bayesian segmentation algorithm based on a probabilistic atlas derived from histology. To obtain the parcellation of the thalamic nuclei at the group level, first, we reconstructed the whole brain T1-weighted image (T1w) of the 178 subjects using the "recon-all" function in the FreeSurfer software (version 7.1.1). The reconstruction step included non-uniform intensity normalization, skull-stripping, and gray/white matter tissue segmentation, etc. (Fischl et al. 2002, 2004). Second, to obtain a more reliable thalamic segmentation, a T2-weighted scan was used as an additional MRI volume with the T1w using the "segmentThalamicNuclei.sh" function with "t2" boundary-based registration mode. Third, we obtained individual segmentation of thalamic nuclei, including the anteroventral nuclei, central medial nuclei, central lateral nuclei, centro-median nuclei, laterodorsal nuclei, lateral/medial geniculate nuclei, lateral posterior nuclei, supra-geniculate, mediodorsolateral parvocellular, mediodorsomedial magnocellular, reuniens, parafascicular, anterior/inferior/lateral/medial pulvinar, and ventral anterior/lateral anterior/lateral posterior/posterolateral nuclei. Fourth, to map the individual thalamic nuclei into the same standard stereotaxic space, a 3-stage (rigid + affine + nonlinear) symmetric normalization (SyN) algorithm implemented in ANTs (Avants et al. 2011) was used to register between each individual's gray matter segment and the gray matter tissue segment of the MNI ICBM 2009c template (mni_icbm152_gm_tal_nlin_asym_09c) (Fonov et al. 2009, 2011). The calculated linear and non-linear transformations were applied to each individual's thalamic nuclei segmentation and then warped into MNI ICBM 2009c nonlinear asymmetric T1 space. Lastly, we conducted a winner-takes-all strategy to label each voxel belonging to a particular thalamic nucleus with the highest probability using the segmentation we performed of the 178 HCP participants for the HCPex atlas, to obtain the final group-level atlas of the thalamic nuclei in the MNI ICBM 2009c standard space.

The FreeSurfer module segmented the thalamus into 25 different nuclei in each hemisphere. However, some of the thalamic nuclei were so small that they might be spatially inaccurate or not practical for further ROI-based analysis. For that reason, we reduced the number of thalamic nuclei by merging small nuclei according to their original definitions or nearest neighbours. Detailed descriptions of the resulting 21 thalamic nuclei that are defined in the HCPex atlas are shown in Table 1.

The thalamic parcellation provided by Iglesias et al (2018) enabled inclusion of 21 thalamic nuclei in each hemisphere in the HCPex atlas, and was accordingly used in preference to an atlas by Tian et al (2020) which provides only 8 thalamic nuclei. The thalamic parcellation adopted from Iglesias et al. al (2018) was validated using the Krauth et al (2010) atlas which is based on histology of the human brain, as described in the Supplementary Material (Fig. S1). For a further validation, the human thalamic nuclei from the Thalamus Optimized Multi Atlas Segmentation (THOMAS) atlas which uses white matter-nulled MP-RAGE imaging that segments the thalamus into 12 nuclei (Su et al. 2019) is also shown in Fig. S1.

Putamen, caudate, nucleus accumbens, globus pallidus externalis/internalis, substantia nigra pars compacta/reticulata, ventral tegmental area, mammillary bodies, septal nuclei, and nucleus basalis

Nine areas were adapted from the reinforcement learning atlas (Pauli et al. 2018), including the putamen, caudate nucleus, nucleus accumbens, globus pallidus externalis, globus pallidus internalis, substantia nigra pars compacta, substantia nigra pars reticulata, ventral tegmental area, and mammillary bodies. The reinforcement learning atlas defined many useful subcortical nuclei, especially for reward learning and decision making, using high-resolution T1- and T2-weighted structural images across 168 typical adults aged between 22 and 35 years old. The provided deterministic labels defined in the same standard MNI ICBM 2009c nonlinear asymmetric template space (Fonov et al. 2009, 2011) were applied directly in the current modified atlas HCPex.

The septal nuclei and nucleus basalis which contain cholinergic neurons were defined by Zaborszky et al. (2008) based on the cytoarchitectonic mapping of histological serial sections. The stereotaxic probabilistic maps of the magnocellular cell groups were then separated into Ch1-2, Ch3, and Ch4 compartments. For the HCPex atlas, the maximum probability maps (MPM) of the Ch compartments in the single-subject MNI standard space that were helpfully made available by Professor Zaborszky were used, in which Ch1-2 are combined in HCPex as the septal nuclei, and Ch3 and Ch4 are combined into the nucleus basalis. The generation of MPM is described in previous studies (Eickhoff et al. 2005, 2006). Zaborszky et al. (2008) combined into one image (ChAll) the MPM for the Ch cell groups by assigning a label to each voxel that had the highest probability or exceeded a threshold of 40% among the 10 brains. Zaborsky et al. normalized the original histological volume

to the single-subject T1 template (colin27) (Holmes et al. 1998). Thus, to map this with the population-averaged MNI ICBM space, we used the SyN algorithm in ANTs (Avants et al. 2011) to register between the brain-extracted single-subject T1 template and the MNI ICBM 2009c asymmetric T1 template. The calculated transformation was applied to the final ChAll map at the group level and normalized to the MNI ICBM 2009c nonlinear asymmetric T1 space. Finally, the normalized map was corrected by removing any voxels located in the white matter such as the anterior commissure.

Results

Figure 1 provides a labelled version of the extended HCP atlas to help the reader identify brain regions in these coronal slices of the human brain. It is noted that some of the small brain structures can appear very small in these coronal slices as they are separated by 8 mm, with one example the septal nuclei that are between MNI coordinate y: 3–10). Tables 1 and 2 provide lists of the brain areas in the atlas. A list of the labels in this reordered list is provided in HCPex_LabelID.mat.

The procedure used to produce the cortical areas in volumetric space for HCPex was usefully validated against a procedure used by Coalson et al (2018) to produce a volumetric version of the HCP-MMP1 atlas, as shown in the Supplementary Material (Fig. S2).

The extended HCP atlas was tested with public brain imaging software, including SPM, FSL, MRIcroGL, the viewer in FreeSurfer (freeview), and has also been made compatible with the AAL3 software. A user guide for installation is provided in the Supplementary Material. The atlas is in volumetric space, with the aim of making it a useful tool for studying the human brain, especially for the reconstruction and analysis of the structural and functional connectome. To facilitate use in different types of investigation, the atlas is provided with two different resolutions, with isotropic voxel size $1 \times 1 \times 1$ mm and $2 \times 2 \times 2$ mm, along with a skull-stripped ICBM 2009c asymmetric T1 template for normalization and visualization.

Users should note that small parcels, such as the nuclei reuniens and limitans of the thalamus (< 10 voxels in the 1 cubic mm version), could be missed after nonlinear normalization in low-resolution fMRI studies. Also, as the cortical and subcortical regions were originally defined based on young adults' brain images, caution should be given in age-related investigations, and visual inspection is suggested.

Data availability

Software and code for the extended HCP atlas The HCPex atlas, including its different versions, labels, code, and the User guide, is available in association with this paper at the authors' websites https://www.oxcns.org and https://github.com/wayalan/HCPex as HCPex.zip.

Discussion

The HCPex atlas described here extends the HCP-MMP1 atlas (Glasser et al. 2016a) by adding 66 subcortical areas, by providing it in volumetric form for use with many types of neuroimaging software including SPM, by providing labelled coronal slices of the brain to provide clear visualization of the cortical and subcortical regions defined in the HCPex atlas (Fig. 1), and by providing an optional reordering of the cortical regions in the atlas (Table 1). We have already found that with these extensions the HCPex atlas is very helpful (Huang et al. 2021; Ma et al. 2021; Rolls et al. 2021).

The parcellation of the thalamus provided in HCPex and AAL3 (Rolls et al. 2020) is similar, but differs in the following respects. AAL3 uses the same approach to segmentation of the thalamic nuclei (Iglesias et al. 2018) as HCPex, but users should note that there are differences in the T1 templates that are applied. The thalamic nuclei in AAL3 are segmented and defined with the single subject colin27 (scanned for 27 times) template images that are linearly registered to the MNI305 space. The segmentation of the thalamic nuclei in HCPex is based on the average template generated by 152 unbiased non-linear averages in the MNI152 database, and is thus less biased by any single subject's anatomical characteristics (Fonov et al. 2011). In addition, the limitans suprageniculate thalamic nuclei are defined in HCPex, and were not included in AAL3.

The HCPex atlas has already proved very useful in an analysis of the connections of the human hippocampal memory system using diffusion tractography (Huang et al. 2021). The atlas enabled the connections of the many visual and related cortical areas so beautifully parcellated in the HCP-MMP atlas with the human hippocampus to be described, but in addition enabled the connections of the hippocampal memory system with other brain areas, such as the para-hippocampal, cingulate and orbitofrontal cortices, to be included in the analysis (Huang et al. 2021). For example, it enabled connections between the hippocampus and HCP atlas areas VMV1-3 and PHA1-3 (i.e. TH), which include the para-hippocampal place area (Sulpizio et al. 2020), to be revealed. This is an important finding, because it helps to elucidate how hippocampal spatial view cells which respond to a viewed location in a scene (Rolls et al. 1997; Georges-François et al. 1999; Rolls and Wirth 2018; Rolls 2021), and so are important in human memory and navigation (Kesner and Rolls 2015; Rolls 2018, 2021), may receive their inputs.

That would not have been revealed by other atlases, because they have less detailed and multimodal parcellation of these brain regions.

Limitations

We note that the areas defined in the HCP-MMP atlas (Glasser et al. 2016a) are defined in a surface-based map, and that this has advantages for accurate registration (Van Essen et al. 2017; Coalson et al. 2018; Dickie et al. 2019). The HCPex atlas described here is in volumetric space, and as described by Coalson et al (2018), a volumetric version may be less accurate than a surface-based version because there is some variability in the cortical folding between different participants which can influence registration in volumetric space. Validation of the HCPex atlas in volumetric space with the volumetric atlas provided by Coalson et al (2018) is provided in the Supplementary Material (Fig. S2), where the methods used to produce these two volumetric atlases are compared. The advantage of the HCPex atlas is that it is extended to include many subcortical areas, and is in volumetric space in a form that is ready used by many neuroimaging analysis programs including but not limited to SPM (https://www.fil.ion.ucl.ac.uk/spm/), FSL (https://fsl.fmrib.ox.ac.uk/fsl/fslwiki), the AAL-AAL3 toolboxes (https://www.gin.cnrs.fr/en/tools/aal/), FreeSurfer (https://surfer.nmr.mgh.harvard.edu/), and MRIcroGL (https://www.mccauslandcenter.sc.edu/mricrogl/home). We suggest that if very accurate identification of cortical areas is needed, then it would be useful to follow any HCPex analysis with an analysis in surface-based space.

In conclusion, the HCPex atlas described here extends the HCP-MMP1 atlas (Glasser et al. 2016a) by adding 66 subcortical areas, by providing it in volumetric form for use with many types of neuroimaging software including SPM, by providing labelled coronal slices of the brain to provide clear visualization of the cortical and subcortical regions defined in the HCPex atlas (Fig. 1), and by providing an optional reordering of the cortical regions in the atlas (Table 1).

Supplementary Information The online version contains supplementary material available at https://doi.org/10.1007/s00429-021-02421-6.

Acknowledgements The use of the HCP-MMP v1.0 atlas (Glasser et al. 2016a, b) in the construction of HCPex is acknowledged, and reference should be made to that paper if use is made of HCPex. The volumetric version of the Glasser et al. atlas (2016a) produced by Coalson et al. (2018) was downloaded with grateful acknowledgement from the publicly released version of the parcellation (https://balsa.wustl.edu/file/show/nvrZ). The neuroimaging data were provided by the Human Connectome Project, WU-Minn Consortium (Principal Investigators: David Van Essen and Kamil Ugurbil; 1U54MH091657) funded by the 16 NIH Institutes and Centers that support the NIH Blueprint for Neuroscience Research; and by the McDonnell Center for Systems Neuroscience at Washington University. Professor Laszlo Zaborszky is warmly thanked for providing a parcellation of the Ch1-Ch4 nuclei based on Zaborszky et al. (2008).

Author contributions C–C Huang and E T Rolls prepared the atlas and wrote the paper. C-P Lin and J.Feng read and approved the paper, and provided funding.

Funding This research was supported by a grant to Professor C-P. Lin that included research with Professor E.T. Rolls (Ministry of Science and Technology (MOST) of Taiwan, MOST 110-2321-B-010-010-004 and MOST 110-2634-F-010-001). The research was also supported by the following grants to Professor J. Feng: National Key R&D Program of China (No. 2019YFA0709502); 111 Project (No. B18015); Shanghai Municipal Science and Technology Major Project (No. 2018SHZDZX01), ZJLab, and Shanghai Center for Brain Science and Brain-Inspired Technology; and National Key R&D Program of China (No. 2018YFC1312904). The funding agencies took no part in the design of this research.

Declarations

Conflict of interest The authors have no conflict of interest to declare.

Ethical Permissions No data were collected as part of the research described here. The data were from the Human Connectome Project, and the WU-Minn HCP Consortium obtained full informed consent from all participants, and research procedures and ethical guidelines were followed in accordance with the Institutional Review Boards (IRB), with details at the HCP website (http://www.humanconnectome.org/).

Software and code for the extended HCP atlas The HCPex atlas, including its different versions, labels, code, and the User guide, is available in association with this paper at the authors' websites https://www.oxcns.org as HCPex_v1.0.zip and https://github.com/wayalan/HCPex.

References

Avants BB, Tustison NJ, Song G (2009) Advanced normalization tools (ANTS). Insight j 2(365):1–35

Avants BB, Tustison NJ, Song G, Cook PA, Klein A, Gee JC (2011) A reproducible evaluation of ANTs similarity metric performance in brain image registration. Neuroimage 54(3):2033–2044. https://doi.org/10.1016/j.neuroimage.2010.09.025

Beauchamp MS (2021) Cortical Surface HCP. https://openwetware.org/wiki/Beauchamp:CorticalSurfaceHCP

Chakravarty MM, Steadman P, van Eede MC, Calcott RD, Gu V, Shaw P, Raznahan A, Collins DL, Lerch JP (2013) Performing label-fusion-based segmentation using multiple automatically generated templates. Hum Brain Mapp 34(10):2635–2654. https://doi.org/10.1002/hbm.22092

Coalson TS, Van Essen DC, Glasser MF (2018) The impact of traditional neuroimaging methods on the spatial localization of cortical areas. Proc Natl Acad Sci USA 115(27):E6356–E6365. https://doi.org/10.1073/pnas.1801582115

Dickie EW, Anticevic A, Smith DE, Coalson TS, Manogaran M, Calarco N, Viviano JD, Glasser MF, Van Essen DC, Voineskos AN (2019) Ciftify: a framework for surface-based analysis of

legacy MR acquisitions. Neuroimage 197:818–826. https://doi.org/10.1016/j.neuroimage.2019.04.078
Eickhoff SB, Stephan KE, Mohlberg H, Grefkes C, Fink GR, Amunts K, Zilles K (2005) A new SPM toolbox for combining probabilistic cytoarchitectonic maps and functional imaging data. Neuroimage 25(4):1325–1335
Eickhoff SB, Heim S, Zilles K, Amunts K (2006) Testing anatomically specified hypotheses in functional imaging using cytoarchitectonic maps. Neuroimage 32(2):570–582. https://doi.org/10.1016/j.neuroimage.2006.04.204
Entis JJ, Doerga P, Barrett LF, Dickerson BC (2012) A reliable protocol for the manual segmentation of the human amygdala and its subregions using ultra-high resolution MRI. Neuroimage 60(2):1226–1235. https://doi.org/10.1016/j.neuroimage.2011.12.073
Fischl B, Sereno MI, Dale AM (1999a) Cortical surface-based analysis. II: inflation, flattening, and a surface-based coordinate system. Neuroimage 9(2):195–207. https://doi.org/10.1006/nimg.1998.0396
Fischl B, Sereno MI, Tootell RB, Dale AM (1999b) High-resolution intersubject averaging and a coordinate system for the cortical surface. Hum Brain Mapp 8(4):272–284. https://doi.org/10.1002/(sici)1097-0193(1999)8:4%3c272::aid-hbm10%3e3.0.co;2-4
Fischl B, Salat DH, Busa E, Albert M, Dieterich M, Haselgrove C, van der Kouwe A, Killiany R, Kennedy D, Klaveness S, Montillo A, Makris N, Rosen B, Dale AM (2002) Whole brain segmentation: automated labeling of neuroanatomical structures in the human brain. Neuron 33(3):341–355. https://doi.org/10.1016/s0896-6273(02)00569-x
Fischl B, van der Kouwe A, Destrieux C, Halgren E, Segonne F, Salat DH, Busa E, Seidman LJ, Goldstein J, Kennedy D, Caviness V, Makris N, Rosen B, Dale AM (2004) Automatically parcellating the human cerebral cortex. Cereb Cortex 14(1):11–22. https://doi.org/10.1093/cercor/bhg087
Fonov VS, Evans AC, McKinstry RC, Almli CR, Collins DL (2009) Unbiased nonlinear average age-appropriate brain templates from birth to adulthood. Neuroimage 47:S102
Fonov V, Evans AC, Botteron K, Almli CR, McKinstry RC, Collins DL, Brain Development Cooperative G (2011) Unbiased average age-appropriate atlases for pediatric studies. Neuroimage 54(1):313–327. https://doi.org/10.1016/j.neuroimage.2010.07.033
Friston KJ, Ashburner JT, Kiebel SJ, Nichols TE, Penny WD (2006) Statistical parametric mapping: the analysis of functional brain images. Academic Press
Georges-François P, Rolls ET, Robertson RG (1999) Spatial view cells in the primate hippocampus: allocentric view not head direction or eye position or place. Cereb Cortex 9:197–212
Glasser MF, Coalson TS, Robinson EC, Hacker CD, Harwell J, Yacoub E, Ugurbil K, Andersson J, Beckmann CF, Jenkinson M, Smith SM, Van Essen DC (2016a) A multi-modal parcellation of human cerebral cortex. Nature 536(7615):171–178. https://doi.org/10.1038/nature18933
Glasser MF, Smith SM, Marcus DS, Andersson JL, Auerbach EJ, Behrens TE, Coalson TS, Harms MP, Jenkinson M, Moeller S, Robinson EC, Sotiropoulos SN, Xu J, Yacoub E, Ugurbil K, Van Essen DC (2016b) The Human Connectome Project's neuroimaging approach. Nat Neurosci 19(9):1175–1187. https://doi.org/10.1038/nn.4361
Holmes CJ, Hoge R, Collins L, Woods R, Toga AW, Evans AC (1998) Enhancement of MR images using registration for signal averaging. J Comput Assist Tomogr 22(2):324–333. https://doi.org/10.1097/00004728-199803000-00032
Horn A (2016a) HCP-MMP1.0 projected on MNI2009a GM (volumetric) in NIfTI format.
Horn A (2016b) MMP 1.0 MNI projections. https://www.neurovault.org/collections/1549/
Huang C-C, Rolls ET, Hsu C-CH, Feng J, Lin C-P (2021) Extensive cortical connectivity of the human hippocampal memory system: beyond the "what" and "where" dual-stream model. Cereb Cortex 31:4652–4669. https://doi.org/10.1093/cercor/bhab113
Iglesias JE, Insausti R, Lerma-Usabiaga G, Bocchetta M, Van Leemput K, Greve DN, van der Kouwe A, Alzheimer's Disease Neuroimaging I, Fischl B, Caballero-Gaudes C, Paz-Alonso PM (2018) A probabilistic atlas of the human thalamic nuclei combining ex vivo MRI and histology. Neuroimage 183:314–326. https://doi.org/10.1016/j.neuroimage.2018.08.012
Jenkinson M, Beckmann CF, Behrens TE, Woolrich MW, Smith SM (2012) FSL Neuroimage 62(2):782–790. https://doi.org/10.1016/j.neuroimage.2011.09.015
Kesner RP, Rolls ET (2015) A computational theory of hippocampal function, and tests of the theory: new developments. Neurosci Biobehav Rev 48:92–147. https://doi.org/10.1016/j.neubiorev.2014.11.009
Krauth A, Blanc R, Poveda A, Jeanmonod D, Morel A, Szekely G (2010) A mean three-dimensional atlas of the human thalamus: generation from multiple histological data. Neuroimage 49(3):2053–2062. https://doi.org/10.1016/j.neuroimage.2009.10.042
Ma Q, Rolls ET, Huang C-C, Cheng W, Feng J (2021) Extensive cortical functional connectivity of the human hippocampal memory system.under review
Mills K (2016) HCP-MMP1.0 projected on fsaverage. figshare. Dataset. https://doi.org/10.6084/m9.figshare.3498446.v2
Pauli WM, Nili AN, Tyszka JM (2018) A high-resolution probabilistic in vivo atlas of human subcortical brain nuclei. Sci Data 5:180063. https://doi.org/10.1038/sdata.2018.63
Pipitone J, Park MT, Winterburn J, Lett TA, Lerch JP, Pruessner JC, Lepage M, Voineskos AN, Chakravarty MM, Alzheimer's Disease Neuroimaging I (2014) Multi-atlas segmentation of the whole hippocampus and subfields using multiple automatically generated templates. Neuroimage 101:494–512. https://doi.org/10.1016/j.neuroimage.2014.04.054
Rolls ET (2018) The storage and recall of memories in the hippocampo-cortical system. Cell Tissue Res 373:577–604. https://doi.org/10.1007/s00441-017-2744-3
Rolls ET (2021) Neurons including hippocampal spatial view cells, and navigation in primates including humans. Hippocampus 31:593–611. https://doi.org/10.1002/hipo.23324
Rolls ET, Wirth S (2018) Spatial representations in the primate hippocampus, and their functions in memory and navigation. Prog Neurobiol 171:90–113. https://doi.org/10.1016/j.pneurobio.2018.09.004
Rolls ET, Robertson RG, Georges-François P (1997) Spatial view cells in the primate hippocampus. Eur J Neurosci 9:1789–1794
Rolls ET, Huang CC, Lin CP, Feng J, Joliot M (2020) Automated anatomical labelling atlas 3. Neuroimage 206:116189. https://doi.org/10.1016/j.neuroimage.2019.116189
Rolls ET, Deco G, Huang CC, Feng J (2021) The effective connectivity of the human hippocampal memory system. Cereb Cortex. https://doi.org/10.1093/cercor/bhab442
Smith SM, Jenkinson M, Woolrich MW, Beckmann CF, Behrens TE, Johansen-Berg H, Bannister PR, De Luca M, Drobnjak I, Flitney DE, Niazy RK, Saunders J, Vickers J, Zhang Y, De Stefano N, Brady JM, Matthews PM (2004) Advances in functional and structural MR image analysis and implementation as FSL. Neuroimage 23(Suppl 1):S208-219. https://doi.org/10.1016/j.neuroimage.2004.07.051
Su JH, Thomas FT, Kasoff WS, Tourdias T, Choi EY, Rutt BK, Saranathan M (2019) Thalamus Optimized Multi Atlas Segmentation (THOMAS): fast, fully automated segmentation of thalamic

nuclei from structural MRI. Neuroimage 194:272–282. https://doi.org/10.1016/j.neuroimage.2019.03.021

Tian Y, Margulies DS, Breakspear M, Zalesky A (2020) Topographic organization of the human subcortex unveiled with functional connectivity gradients. Nat Neurosci 23(11):1421–1432. https://doi.org/10.1038/s41593-020-00711-6

Treadway MT, Waskom ML, Dillon DG, Holmes AJ, Park MTM, Chakravarty MM, Dutra SJ, Polli FE, Iosifescu DV, Fava M, Gabrieli JDE, Pizzagalli DA (2015) Illness progression, recent stress, and morphometry of hippocampal subfields and medial prefrontal cortex in major depression. Biol Psychiatry 77(3):285–294. https://doi.org/10.1016/j.biopsych.2014.06.018

Van Essen DC, Smith J, Glasser MF, Elam J, Donahue CJ, Dierker DL, Reid EK, Coalson T, Harwell J (2017) The Brain Analysis Library of Spatial maps and Atlases (BALSA) database. Neuroimage 144(Pt B):270–274. https://doi.org/10.1016/j.neuroimage.2016.04.002

Zaborszky L, Hoemke L, Mohlberg H, Schleicher A, Amunts K, Zilles K (2008) Stereotaxic probabilistic maps of the magnocellular cell groups in human basal forebrain. Neuroimage 42(3):1127–1141. https://doi.org/10.1016/j.neuroimage.2008.05.055